GEOPHYSICS, VOL. 41, NO. 6A (DECEMBER 1976), P. 1184–1206, 21 FIGS., 1 TABLE

EARTH CONDUCTIVITY DETERMINATIONS EMPLOYING A SINGLE SUPERCONDUCTING COIL

H. F. MORRISON,* WILLIAM DOLAN,‡ AND ABHIJIT DEY*

A low-frequency airborne electromagnetic prospecting method has been developed which exploits the inherent low resistance of a superconducting coil. Changes in the input resistance of this coil are monitored in the presence of the conducting earth. The response of the system, the change in the input resistance, is proportional to the quadrature secondary magnetic field at the transmitter, although unlike two-coil systems, the response does not decrease with increasing frequency.

This research has demonstrated that superconducting wires, large scale nonmetallic cryostats, the requisite measurement circuitry, and an appropriate data acquisition system are realizable in a practical flight configuration.

The unicoil presents the following significant advantages in electromagnetic prospecting:

1) The measurement sensitivity is not limited by the relative coil motion experienced by two-coil systems.
2) Ample field strength may be supplied to override ambient noise.
3) Optimum frequencies for specific geologic sections are easily implemented in the range of 10 to 2000 Hz.
4) Maps of ground conductivity may be obtained because precise thermal stability is maintained and the measurement, therefore, is absolute.
5) The point source observation minimizes analytic complexity.
6) The combination of the foregoing features with multiple frequency operation, yields a system of potentially high sensitivity and unprecedented depth of exploration.

The unicoil system also possesses some disadvantages: 1) An operational complexity results from the cryogenic procedures required in the field, and 2) the heavy sensor requires a large helicopter.

INTRODUCTION

An investigation was initiated in 1971 by the Engineering Geoscience group of The University of California at Berkeley on the applications of superconductivity to airborne geophysical exploration. The study was designed to consider the use of superconducting coils to generate low-frequency electromagnetic fields. Investigation of the potential application of superconducting, or Josephson effect, magnetometers as ultra-sensitive detectors for these low-frequency fields was included. The objective was to develop a measurement system offering efficient operation and significantly increased depth of exploration.

It was anticipated that superconducting coils could be developed yielding exceptionally large dipole moments; i.e., that the turns N, current I, and area A product could be made arbitrarily large. Existing airborne electromagnetic dipole transmitters rely either on multiturn solenoids with high permeability cores or on coils of large area. In both cases, the maximum achievable dipole moment is limited by the weight of the coil and by practical power supplies.

Paper presented at the 43rd Annual International SEG Meeting, October 23, 1975 in Mexico City. Manuscript received by the Editor September 22, 1975; revised manuscript received July 11, 1976.
* University of California, Berkeley, Calif. 94720.
‡ Amax Exploration Inc., Denver, Colo. 80212.
© 1976 Society of Exploration Geophysicists. All right reserved.

Direct current tests of superconducting wire showed that current densities of up to 10^5 amp/cm^2 were feasible. Hence, even with the weight of an insulating cryostat, it appeared that moment improvements of several orders of magnitude might be obtained with a coil compatible with a suitable airplane or helicopter.

Ground prospecting systems were also considered. The existing systems rely on horizontal loops up to 1 km in diameter, long grounded wires, or, in the case of shallower prospecting, vertical loops arranged on tower-like structures. On the ground, the moment NIA can be increased arbitrarily by increasing the area A and moments of up to 10^9 amp-turns-m^2 have been obtained. However, the cumbersome field logistics have tended to restrict the development of practical systems, particularly for deep exploration for hydrocarbon and geothermal reservoirs. Superconducting transmitters have the potential of satisfying these requirements with relatively compact multiturn loops that can be easily transported and oriented. With these considerations in mind a low-frequency transmitter is being developed using a rotatable direct current superconducting coil.

Unfortunately, the zero resistance property of a superconductor is manifested only for direct current, and alternating current produces a loss phenomenon. Initial efforts were directed toward experimentally defining the nature of the losses, and design criteria resulted for coils that produce the maximum moment with minimum loss.

While these experiments were in progress, an analysis of existing airborne and ground electromagnetic prospecting systems was performed. In these studies the response of a sphere in free space was used to compare towed bird, towed boom, and aircraft-mounted transmitter-receiver combinations. As realized by many other workers (e.g., Ward, 1967, 1970), it was found that the limiting sensitivity was set by the orientation error between the transmitter and receiver and that, without very elaborate position monitoring or control, increased transmitter moment was not particularly advantageous.

During the course of this investigation, it was realized that the unique advantage of superconductivity lay in the use of a single coil system in which the input impedance of the transmitter is the measured quantity rather than the mutual impedance of a transmitter-receiver pair (Morrison, 1974). The single coil concept (unicoil) was not original, having been proposed originally by Carlson and Hanson (1919) and, subsequently, described theoretically by Sommerfeld (1949), Wait (1953), Negi (1961), and Bhattacharyya (1963). Unicoil systems are presently used in mine detectors, metal locators, and borehole induction logging instruments. The practical systems that have been proposed or implemented monitor the changes in inductance brought about by nearby conductors. Rapid attenuation with increasing distance from the coil renders inductance changes immeasurable if the influencing conductor is much more than a few coil diameters removed.

The resistance of the coil is also modified by a nearby conductor. For a conventional multiturn coil, the effect is no more measurable than the induction effect. However, if the coil is superconducting, the apparent resistance change resulting from a nearby conductor is essentially the only resistance measurable. Hence, a superconducting single coil serves as a very sensitive element for detection of conductors, and detection distances well beyond the range of the inductance measuring devices are feasible. The orientation errors of the transmitter-receiver pair style of measurement are eliminated and the moment can be made large. Flexing or distortions of the coil have a first order effect on its inductance but only a second order effect on the length of the wire and, hence, on its resistance. Additionally, and of major importance from a practical point of view, is the fact that the superconducting coil is a thermally stable circuit element.

The unicoil electromagnetic system will be described in three sections: (1) theory of the unicoil measurement including a comparison of its sensitivity with conventional measurement systems; (2) summary of the theory and practical behavior of superconductors in ac applications; and (3) results of an experimental program designed to yield a practical prospecting device.

THEORY

Introduction

Existing electromagnetic (EM) geophysical prospecting systems consist of a transmitting loop and a receiving coil at some distance from the transmitter. The transmitted field induces eddy currents in the ground and the receiver measures the secondary fields from those induced currents. Variations in application include: (1) both the

transmitter and the receiver on the surface; (2) the transmitter and receiver mounted on an aircraft; (3) the receiver towed behind an aircraft, with either the transmitter on the ground or on the aircraft; (4) the transmitter and receiver mounted together on a frame towed beneath an aircraft; and (5) transmitter and receiver on separate aircraft. With the exception of transient field systems, the secondary field is necessarily observed in the presence of the much larger primary field. Detailed reviews of these systems have been presented by Ward (1967, 1970) and Grant and West (1965) among others.

Two-coil analysis

To analyze two-coil systems, it is convenient to consider the conceptual schematic representation of Figure 1 (after Ward, 1970). A buried conductor, or the ground itself, responds like a shorted resistive secondary of the equivalent transformer. Receiver signals are actually a measure of the mutual impedance of the transmitter-receiver system in the presence of an additional shorted secondary. Following Ward (1970) and the notation of Figure 1, the current induced in the transformer equivalent of the conductor is (assuming an $e^{i\omega t}$ time dependence),

$$I_C = \frac{-i\omega I_T M_{TC}}{R + i\omega L} = \frac{-M_{TC} I_T(\omega^2 L + i\omega R)}{R^2 + \omega^2 L^2}.$$

The current then induces a voltage in the receiver coil V_{CR}, where

$$V_{CR} = -M_{CR}\, i\omega I_C = \frac{i\omega M_{CR} M_{TC} I_T(\omega^2 L + i\omega R)}{R^2 + \omega^2 L^2}.$$

The primary field also induces a voltage in the receiver V_{TR}, where

$$V_{TR} = -M_{TR}\, i\omega I_T,$$

so that the secondary induced voltage may be expressed as a fraction of the primary voltage, i.e.,

$$\frac{V_{CR}}{V_{TR}} = -\frac{M_{CR} M_{TC}}{M_{TR}} \cdot \frac{\omega^2 L + i\omega R}{R^2 + \omega^2 L^2}.$$

It will be seen that this ratio consists of an in-phase and quadrature component referenced to the transmitter current and that both these components go to zero at low frequency. The quadrature component increases to a maximum and at high frequency assumes a $1/\omega$ dependence whereas the in-phase component asymptotes to a constant value.

Unicoil analysis

With this transformer analogy established, we can now analyze the single coil (unicoil) system, shown in Figure 1. A current I_c is induced in the conductor as before. Now, however, we consider the fact that this current induces a voltage back in the transmitter coil

$$V_{CT} = -M_{TC}\, i\omega I_c$$

$$= -\frac{M_{TC}^2 \omega^2 I_T}{R + i\omega L} = -\frac{M_{TC}^2 \omega^2 I_T(R - i\omega L)}{R^2 + \omega^2 L^2}.$$

The secondary in-phase voltage is in opposition to the current flow in the transmitter and, hence, is in opposition to the in-phase voltage across the transmitter. This secondary in-phase voltage may be considered equivalent to an increase of resistance of the coil (if the transmitter current is held constant), i.e.,

$$I_T \Delta R_T = \frac{M_{TC}^2 \omega^2 I_T R}{R^2 + \omega^2 L^2}.$$

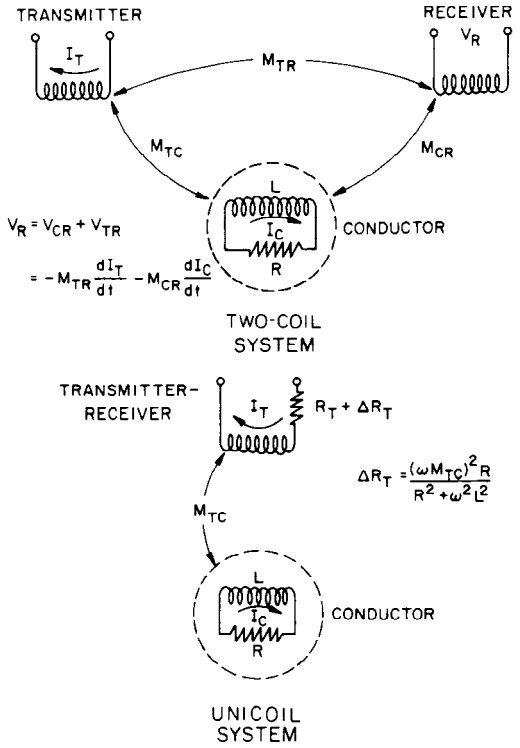

FIG. 1. Transformer representations for two-coil and unicoil EM measurements.

The quadrature voltage may be considered equivalent to a change in inductance of the coil, i.e.,

$$i\omega\Delta L_T I_T = \frac{i\omega^3 M_{TC}^2 L I_T}{R^2 + \omega^2 L^2}.$$

The signal voltages increase linearly with frequency in the case of the quadrature component and reach a constant value in the case of the in-phase.

Closed loop target

When the buried body can be represented by a small coil or, when a small coil is used as a test target, the mutual impedance can be replaced by actual parameters of the coil. For example, if we consider the transmitter to consist of N_1 turns of area A_1 and current I_1, then the magnetic field at the test coil (perpendicular to the plane of the test coil) may be written as $N_1 A_1 I_1 F_{12}$, where F_{12} is a geometric factor describing the appropriate component of the dipole field of the transmitter at the test coil. This field produces an emf in test coil V_2, where

$$V_2 = -N_2 \frac{d\phi}{dt}$$

$$= -N_2 A_2 i\omega N_1 A_1 I_1 F_{12}.$$

(μ has been absorbed in the geometric factor F here and in the following equations; N_2 and A_2 are the turns and area of the test coil.) This voltage will be balanced by the induced current I_2; i.e.,

$$V_2 + I_2 R_2 + i\omega L_2 I_2 = 0,$$

or

$$I_2 = \frac{i\omega N_1 N_2 A_1 A_2 I_1 F_{12}}{R_2 + i\omega L_2}.$$

This current flowing in N_2 turns of area A_2 then produces a field back at the transmitter of

$$H = N_2 A_2 I_2 F_{21}$$

$$= \frac{i\omega(N_2 A_2)^2 (N_1 A_1) F_{21} F_{12} I_1}{R_2 + i\omega L_2}$$

$$= \frac{(N_2 A_2)^2 (N_1 A_1) F_{21} F_{12} (\omega^2 L_2 + i\omega R_2) I_1}{R_2^2 + \omega^2 L_2^2}.$$

This last expression is of the form

$$f(N_1 A_1\ N_2 A_2)(M + iN) F_{21} F_{12},$$

or a constant of the transmitter and target, multiplied by a response function, and by a geometric factor. This is the way most electromagnetic target responses are written. For example, a small sphere of radius a in a uniform magnetic field H_0 produces a secondary field given by

$$\Delta H = H_0 a^3 (M + iN) F,$$

where F is the geometric factor describing this secondary dipole field at the point where ΔH is observed. The small coil analogy above shows that M, called the in-phase response, is equivalent to

$$\frac{\omega^2 L_2}{R_2^2 + \omega^2 L_2^2},$$

and N, the quadrature component, is equivalent to

$$\frac{\omega R_2}{R_2^2 + \omega^2 L_2^2}.$$

For our later discussion it is instructive to pursue this analogy. Figure 2 shows the functions M and N for a sphere as a function of the induction number θ. [$\theta = (\sigma\,\omega\,\mu)^{1/2} a$; σ is the conductivity, μ the permeability, and a is the radius of the sphere.] The equivalent functions for the small loop behave in a similar fashion as a function of frequency for fixed R and L. Both start at zero for zero frequency, the in-phase response asymptotes to a constant value as frequency increases while quadrature decreases again to zero at infinite frequency.

Returning to the coil representation of the single coil response to a nearby conductor, we see that this secondary field will induce a voltage in the transmitter of:

$$\Delta V = -N_1 \frac{d\phi}{dt},$$

or

$$\Delta V = -\mu i\omega N_1 A_1 H$$

$$= \mu\omega^2 \frac{(N_1 A_1)^2 (N_2 A_2)^2 F_{12} F_{21} I_1 (R_2 - i\omega L_2)}{R_2^2 + \omega^2 L_2^2}$$

$$= I_1 \Delta R_1 + i\omega I_1 \Delta L_1.$$

Then the change in resistance observed in the transmitter becomes

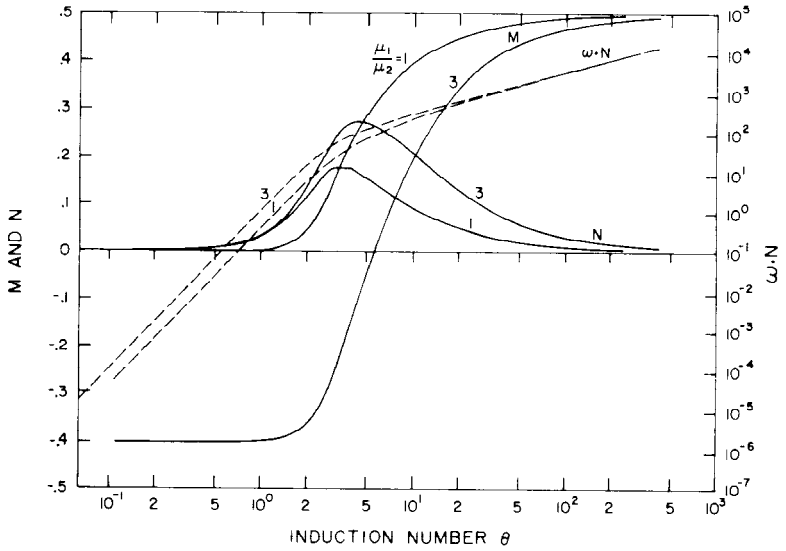

FIG. 2. Normalized EM response of a spherical conductor.

$$\Delta R_1 = \frac{\mu(N_1A_1)^2\,(N_2A_2)^2\,F_{21}\,F_{12}\,\omega^2\,R_2}{R_2^2 + \omega^2\,L_2^2},$$

and the change in inductance becomes

$$\Delta L_1 = \frac{\mu(N_1A_1)^2\,(N_2A_2)^2\,F_{21}\,F_{12}\,\omega^2\,L_2}{R_2^2 + \omega^2\,L_2}.$$

If the properties of the target remain constant and the geometry remains constant, then it can be seen that the amplitude of the resistance and inductance change is proportional to the square of the (NA) product of the transmitter.

It is now evident that the quadrature component of the secondary field is responsible for the change in resistance, and the in-phase secondary field causes changes in the inductance. Further, it can be seen from these last expressions that both ΔR and ΔL should now asymptote to a constant value at high values of ω. The values of ΔR, if the response of a sphere is substituted, are proportional to ωN and this function is plotted in Figure 2.

It should be noted that the quasi-static assumptions under which the M and N curves are calculated are invalid at frequencies substantially higher than those with which we are concerned.

Unicoil quadrature behavior

An extremely important point has been demonstrated by the equations developed thus far. The two-coil measurement involves normalizing the secondary signal with the primary signal, i.e.,

$$\frac{V_{\text{secondary}}}{V_{\text{primary}}} = \frac{V_{CR}}{V_{TR}} = K(M + i\,N),$$

where K = the geometric constant, and M and N are the in-phase and quadrature components, respectively, reflecting the electrical parameters of the conductor. The unicoil measurement is inherently an absolute measurement independent of transmitter coil current and is, consequently, not normalized; i.e.,

$$V_{\text{secondary}} = V_{CT} = K_1(M_1 + i\,N_1),$$

where K_1 = the geometric constant and M_1 and N_1 are the in-phase and quadrature components, respectively, reflecting the electrical parameters of the conductor and are not the same as the M or N above.

The following table shows this comparison, using the small test coil as the target;

	In-Phase	Quadrature
Two-coil	$M = \dfrac{\omega^2 L}{R^2 + \omega^2 L^2}$	$N = \dfrac{\omega R}{R^2 + \omega^2 L^2}$
Unicoil	$M_1 = \dfrac{\omega^2 R}{R^2 + \omega^2 L^2}$	$N_1 = \dfrac{\omega^3 L}{R^2 + \omega^2 L^2}$

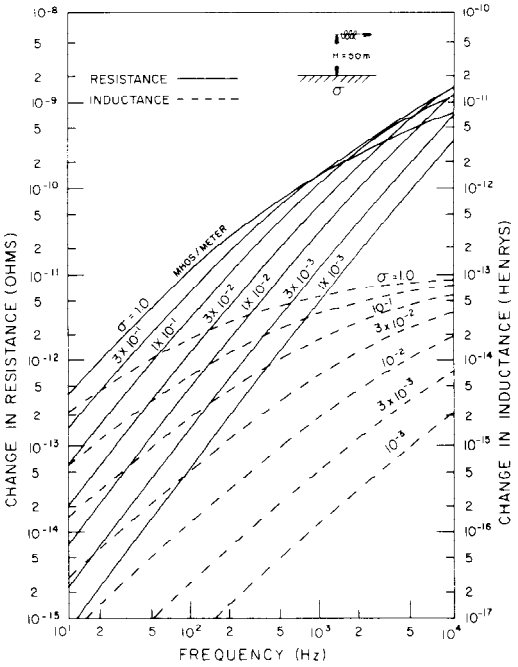

FIG. 3. Unicoil response to a conducting half-space; constant height with frequency and conductivity variable.

A traditional concern with two-coil quadrature systems is that highly conducting ore bodies will be missed (note the N behavior in Figure 2). In the unicoil system, the in-phase secondary voltage equates to the quadrature magnetic field. However, its behavior is similar to the in-phase response in the two-coil system. Accordingly, there is no likelihood of failing to detect good conductors. This is especially true in view of recent results which show an enhanced quadrature secondary magnetic field due to the presence of conductive host rock (Gaur et al, 1972).

From the simple coil analogy it is seen how the impendance changes in the unicoil are calculated for any nearby conductor. The vector component of the secondary field along the axis of the transmitter is calculated at the transmitter location and is converted to the change in resistance and inductance. The calculations are made, assuming that the NA of the transmitter is unity and that the secondary field is uniform over the area of the transmitting coil. Any arbitrary transmitter can be analyzed by multiplying by the appropriate value of $(NA)^2$.

The loop used above to represent a buried conductor provides an excellent target for testing EM systems. Single turn loops of appropriate radius and resistance laid out on the ground and equipped with a closure switch have been used to test the sensitivity of a prototype unicoil system and these results are reported later in the paper.

Unicoil half-space response

The secondary fields of an elevated dipole of moment NIA over a uniform half-space were calculated using standard analyses (Dey and Ward, 1971; Ryu et al, 1971). The ΔR and ΔL of the unicoil were calculated assuming NA to be unity.

Values of ΔR and ΔL for a horizontal dipole transmitter are plotted as a function of frequency for various ground conductivities at a constant height in Figure 3. It can be seen that for practical ranges of conductivity and frequency the response for the quadrature field ΔR continues to increase with frequency as discussed above. Values of ΔR and ΔL are plotted versus height for various frequencies for a constant ground conductivity in Figure 4.

Unicoil orientation effects

For half-space models, the values of ΔR and

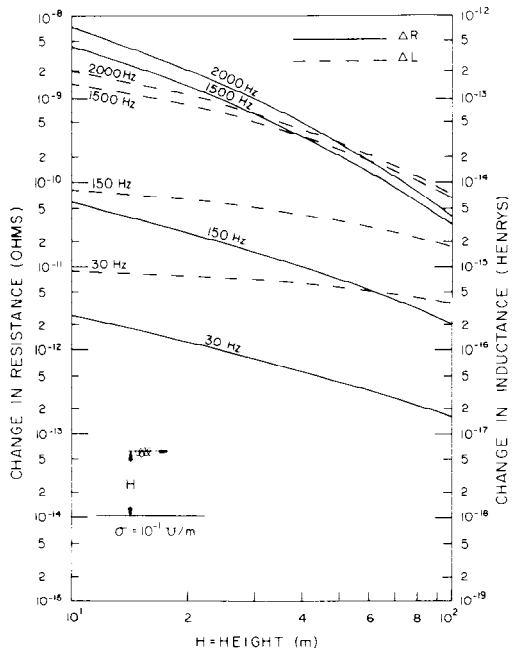

FIG. 4. Unicoil response to a conducting half-space; constant conductivity with frequency and height variable.

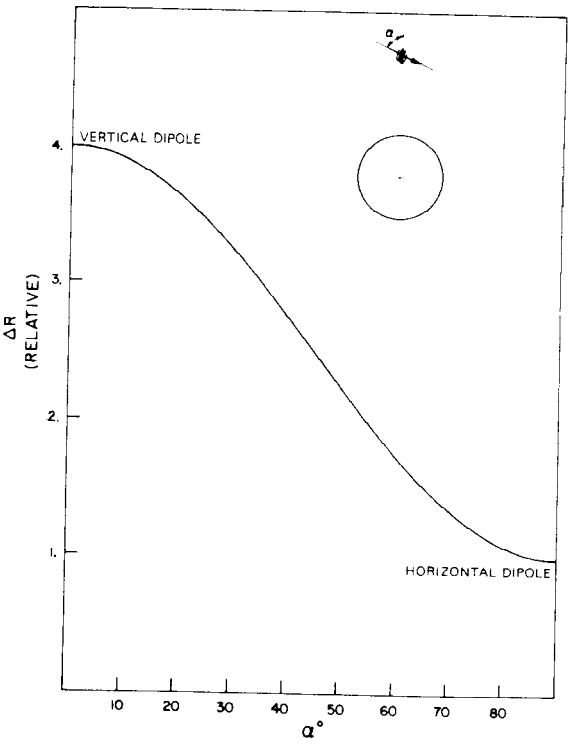

FIG. 5. Plot of orientation function, $2\cos\alpha + \sin\alpha$ of unicoil response of a sphere.

ΔL for a vertical dipole are exactly twice that for the horizontal dipole in the same location. For our simple treatment of the response of a sphere, or a target loop whose orientation is always maximum-coupled to the transmitted field, the response for a coaxial orientation is four times that of a coplanar orientation response. The result is important in considering the orientation noise of the system. As the transmitter dipole rotates through an angle α from vertical to horizontal over a sphere, the value of ΔR has the functional behavior plotted in Figure 5. It is evident that the transmitter sees very little change in resistance over a sphere for small changes in orientation; there is about a 2.5 percent change in ΔR for a 10 degree change from vertical.

Unicoil sphere response

The values of ΔR and ΔL calculated for a vertical coil over spheres of 20 and 100 m radii and of conductivity 10 mhos/m are shown in Figures 6 and 7. The values were obtained by first calculating the vector primary field of the transmitter at the center of the sphere. This field was then assumed to be a uniform field across the entire sphere and the response was calculated following the standard method described by Wait (1951) or Ward (1959). The component of the secondary field perpendicular to the plane of the transmitter coil and at the center of the transmitter was then used to calculate the ΔR and ΔL values. This approach results in a significant error if the radius of the sphere is comparable to the distance from its center to the transmitter. However, for comparison of the unicoil response with that of two-coil systems, it is primarily important that the same model calculation approach be employed.

A practical unicoil system

Large $(NA)^2$ and low, thermally stable resistance can make the unicoil system practical. Since high $(NA)^2$ implies a high inductance, very small changes in inductance caused by the in-phase secondary magnetic fields are undetectable. The unicoil system with a vanishing inherent coil resistance will thus only be able to detect the quadrature secondary magnetic field which is reflected by a change in the coil resistance. Nonetheless, as stated earlier, this style of quadrature ob-

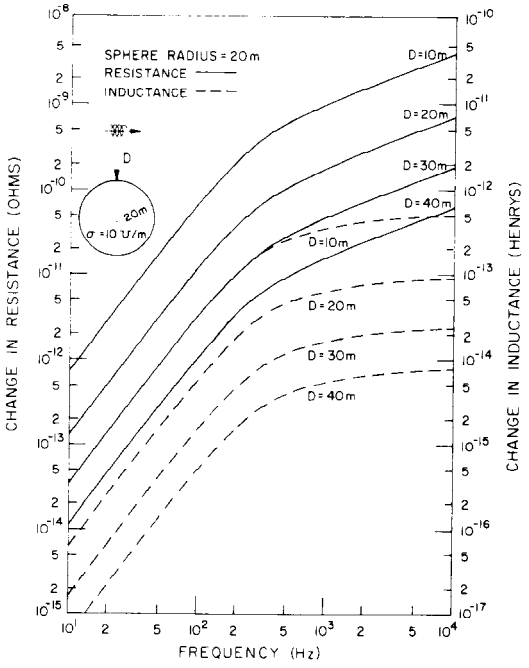

FIG. 6. Unicoil response diagram, sphere, radius 20 m, σ = 10 mhos/m.

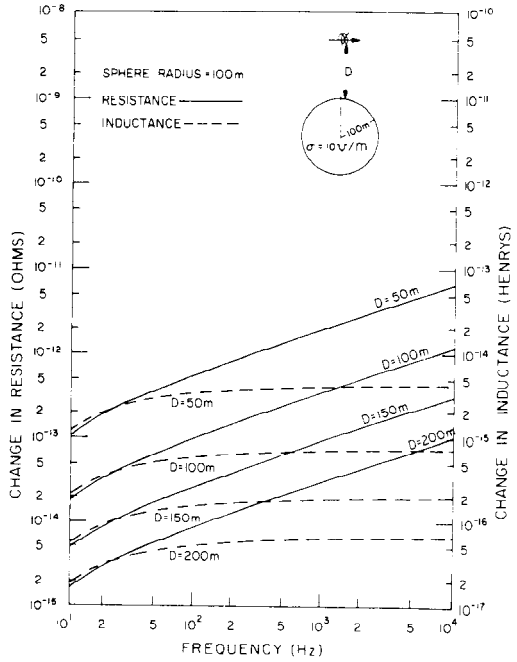

FIG. 7. Unicoil response diagram, sphere, radius 100 m, σ = 10 mhos/m.

servation is not restrictive as in the case of most two-coil systems.

Superconducting coils do allow the required $(NA)^2$ and also possess the needed low resistance. In addition, the low resistance permits coil operation at large dipole moments which assures good signal-to-noise ratios; this is an important consideration since the large NA product implies good detection of natural electromagnetic noise fields. The inherent thermal stability of the supercooled coil is an important factor in realizing the required measurement sensitivity. Finally, the resistance of the coil, dependent on the length of the wire, is relatively unaffected by the small mechanical deformations expected in the coil-cryostat system.

Unicoil versus two-coil systems

A quantitative theoretical comparison of the unicoil system with other electromagnetic prospecting systems is presently possible only for relatively simple models. Mathematical models that can provide the electromagnetic response of a conductive body within a conductive half-space to an elevated dipole source have only recently been achieved (Hohmann, 1975). These techniques, and their computer algorithms, are not yet available for routine analysis. Therefore, the only recourse for comparison is to treat models of simple shape in free space.

We have chosen to use spheres for the comparison. The sphere is a difficult target in a real geologic setting, compared to tabular bodies, and that makes it useful for comparative tests. Four two-coil EM systems were "flown" over two spheres at various elevations of the receiver above the top of the sphere and at three frequencies. The model spheres had conductivities of 10 mhos/m and radii (R) of 20 and 100 m. The depth (D) of the top of the sphere from the receiver (in the two-coil systems) or from the unicoil was varied from 60 to 260 m.

The four two-coil configurations were: (1) The coplanar transverse system with 20 m transmitter-receiver separation; (2) the coaxial boom or a towed boom system with a 10 m separation; (3) the quadrature system having the receiver towed 130 m horizontally behind a horizontal loop transmitter and at an angle of 30 degrees below the horizontal; and (4) the Input transient system.

The results for the frequency domain systems are presented in Table 1. For the rigid mounted systems, the secondary fields at the receiver are indicated. For the towed bird system, the phase angle of the vertical and horizontal fields is presented. Representative noise levels are 20 ppm for the transverse coplanar system (Ward, 1970), 4 ppm for the coaxial boom system (Fraser, 1972) and 0.05 degrees for the towed bird system (G. H. McLaughlin, 1970, personal communication). For the unicoil system, the maximum change in resistance in the transmitter is given assuming an NA of one. For a particular coil this value must be multiplied by the appropriate $(NA)^2$. This value can then be expressed in parts per million of the normal circuit resistance of the system in free space.

The maximum sensitivity of two-coil systems is limited by coupling noise generated by motion of the receiver with respect to the transmitter. With this source of error eliminated, we can conservatively assume that changes in resistance on the order of 1 ppm can be resolved with the unicoil system using conventional electronic procedures.

It is useful to anticipate the realizable characteristics of a superconducting unicoil described in the next section. We may assume, at 100 Hz, a system with a moment (NIA) of 5×10^4 and a

Table 1. Comparison of single coil and two coil prospecting systems.

System	Coaxial (towed boom)		Transverse coplanar		Towed receiver Horizontal	Vertical	Unicoil (Na = 1)		Test sphere	
Frequency Hz	In-phase ppm	Quadrature ppm	In-phase ppm	Quadrature ppm	Phase	(degrees)	ΔL (henries)	ΔR (ohms)	R (m)	D (m)
100	0.4	1.4	6.6	22.4	0.05	0.22	8.78×10^{-17}	1.84×10^{-13}	20	60
320	2.3	2.5	37.4	41.1	0.10	0.40	4.91×10^{-16}	1.08×10^{-12}	20	60
1600	5.0	1.7	81.8	27.8	0.07	0.27	1.07×10^{-14}	3.67×10^{-12}	20	60
100	0.6	0.2	9.8	2.6	0.04	0.32	1.23×10^{-16}	2.04×10^{-14}	100	160
320	0.7	0.1	11.2	1.6	0.02	0.20	1.40×10^{-16}	3.96×10^{-14}	100	160
1600	0.8	0.04	12.1	0.7	0.01	0.09	1.52×10^{-16}	9.32×10^{-14}	100	160
100	0.2	0.06	3.4	0.9	0.01	0.14	4.29×10^{-17}	7.11×10^{-15}	100	210
320	0.2	0.03	3.9	0.6	0.01	0.08	4.88×10^{-17}	1.38×10^{-14}	100	210
1600	0.3	0.02	4.2	0.3	0.004	0.04	5.30×10^{-17}	3.05×10^{-14}	100	210
100	0.09	0.02	1.4	0.4	0.006	0.06	1.75×10^{-17}	2.90×10^{-15}	100	260
320	0.1	0.01	1.6	0.2	0.004	0.04	1.95×10^{-17}	5.62×10^{-15}	100	260
1600	0.1	0.00	1.7	0.1	0.002	0.02	2.16×10^{-17}	1.32×10^{-14}	100	260

D = Depth to top of sphere from receiver (m) R = Radius of sphere (m)

$(NA)^2$ of 3×10^8. A circuit resistance of 0.3 ohms and a measurement sensitivity of 1 ppm will yield detection of resistance changes of 3×10^{-7} ohms. Let us then consider this capability for detecting a 100 m radius sphere at a depth of 210 m (to its top) at a frequency of 100 Hz. From Table 1, the response for a vertical transmitter will be $(NA)^2 \times 7.11 \times 10^{-15}$, or 21.33×10^{-7} ohms. In a circuit of resistance .3 ohms (again anticipating the next section) this is a signal of 7.11 ppm—as stated above, this represents a signal-to-noise (S/N) ratio of 7.11.

Considering the noise levels given above for the other systems, the unicoil is more sensitive. At 320 Hz the coaxial system has a S/N ratio of .03, the coplanar a S/N of 0.2, and the towed bird system a S/N of 1.6. It is not practical to operate them at 100 Hz, hence, noise figures do not exist.

Becker's ratio comparison

An alternate approach to the comparison with other systems has been suggested by Alex Becker (personal communication, 1974). He considered a conventional helicopter coaxial, two-coil system operating at the same frequency as the unicoil system, and with a coil separation of 10 m. With such short separation, the ratio of secondary field to transmitter moment can be considered similar when the distance to a conductor is large relative to the two-coil separation. Thus, the ratio of the unicoil secondary field H_u to the helicopter secondary field H_2 is

$$\frac{H_u}{H_2} = \frac{(NIA)_u}{(NIA)_2} .$$

Now the helicopter primary field at the receiver is given by

$$H_2^{\circ} = \frac{(NIA)_2}{2\pi\rho^3} ,$$

where ρ is the coil separation. We find, therefore, $(NIA)_2 = 2\pi\rho^3 H_2^{\circ}$. Then we have

$$H_u = \frac{H_2}{H_2^{\circ}} \frac{(NIA)_u}{2\pi\rho^3} . \qquad (A)$$

Now, as stated above the change in resistance of the unicoil may be related to the quadrature component of the secondary field, H_u^Q, by

$$I\Delta R = \mu\omega\, NA\, H_u^Q .$$

If we now substitute for the single coil field as expressed by (A) above, we obtain

$$\Delta R = \frac{\omega\mu(NA)^2}{2\pi\,\rho^3} \frac{H_2^Q}{H_2^{\circ}} .$$

The inductance of the single coil is given approximately by (Terman, 1943)

$$L \simeq \frac{1.575\, N^2 r \times 10^{-5}}{3 + 19c/2r} ,$$

where c is the axial length. In our case c is much less than $2r$, so

$$L \simeq 5.25\, N^2 r \times 10^{-6} \text{ henries.}$$

If we now express the $(NA)^2$ product of the single coil in terms of its inductance L and radius r

$$\mu(NA)^2 \simeq 2.36\, r^3 L,$$

and if we divide both sides of the equation for ΔR by the intrinsic resistance of the coil R, we obtain

$$\frac{\Delta R}{R} = .376 \left(\frac{r}{\rho}\right)^3 \left(\frac{\omega L}{R}\right) \left(\frac{H_2^Q}{H_2^\circ}\right).$$

Again anticipating the results of the next section $\omega L/R$, the Q of the coil is conservatively about 5000. With r of 1.6 m and ρ of 10 m, we obtain

$$\frac{\Delta R}{R} = 6.34\, \frac{H_2^Q}{H_2^\circ}.$$

The single coil anomaly is thus more than 6 times the anomaly from the helicopter system.

It should be noted that another significant advantage provided by the unicoil system is that there is not a practical lower limit on the frequency. There has long been motivation to operate a full order of magnitude lower in frequency than existing systems. The premise has been simple. From skin depth $(\sigma\omega\mu/2)^{-1/2}$ considerations alone, it can be seen that the depth of exploration in conductive terrain will be increased. Lower frequencies will be useful in existing mining districts in the search for large deposits at depth. Two-coil systems essentially have power requirements proportional to $1/\omega^2$ and, accordingly, frequencies below 150 Hz are practically prohibitive.

It is commonly realized that multiple frequency operation is required for optimal analysis of electromagnetic prospecting information. The unicoil field system being developed under this program actually uses three frequencies which can be readily adjusted for specific geologic situations.

Unicoil versus Input

Finally, for a comparison with the Input transient system, a computer realization of the Input response over the same spheres was obtained. The geometric configuration of the transmitter (horizontal loop), receiver (vertical Hx and horizontal Hz) and sphere, the transmitter wave shape, and an example of the profile response from the multiple channels over one of the spheres is included, with a summary of the model results, in Figure 8. The channel values in this system are actually average values for the indicated time window and they are expressed as a fraction (parts per million) of the peak-to-peak voltage seen by the receiver during the on-time of the pulse. As a representative example, the 100 m radius sphere discussed above at a depth below the receiver of 210 m produces an Input response of 5 ppm on channel 1. Considering that conservative estimates of the operational noise level range from 40 to 160 ppm, this sphere would not be detectable. The unicoil system had an S/N ratio of over 7 for this same sphere at 100 Hz. At 30 Hz, the unicoil still offers an S/N ratio of over 4.

AC SUPERCONDUCTORS

Introduction

Certain metals such as niobium, tin, lead, and a host of metal alloys have been shown to have the property of zero electrical resistance to direct current at temperatures near absolute zero. Wires made of these metals can carry very large currents, and very large dc electromagnets have been built in this way.

Another basic property of superconductors is that magnetic fields are expelled from the interior. At very high magnetic field strengths the field does enter the wire and destroys the superconductivity. In some superconductors, called type 1, such as lead or tin, the magnetic field enters the metal rapidly and penetrates throughout. The transition from superconducting to normal state that accompanies this field penetration is equally rapid and complete. The magnetic field causing this transition is called the critical field and for all type 1 materials the value is less than 2000 gauss. In type 2 superconductors the penetration takes place gradually over a certain interval. Fields first enter at a lower critical field strength of as little as several hundred gauss, but the conductivity transition may not occur until fields as high as 400,000 gauss are reached. It appears that the field enters the material as individual or quantized lines of magnetic flux in the vicinity of which the material is a normal conductor. When the density of these flux lines reaches a certain critical level, there is no more superconductor free of flux lines and the superconductivity disappears.

In a wire carrying current the magnetic field is the self field of the wire. As the current is increased the field at the surface of the wire also increases (according to Ampere's law) and upon

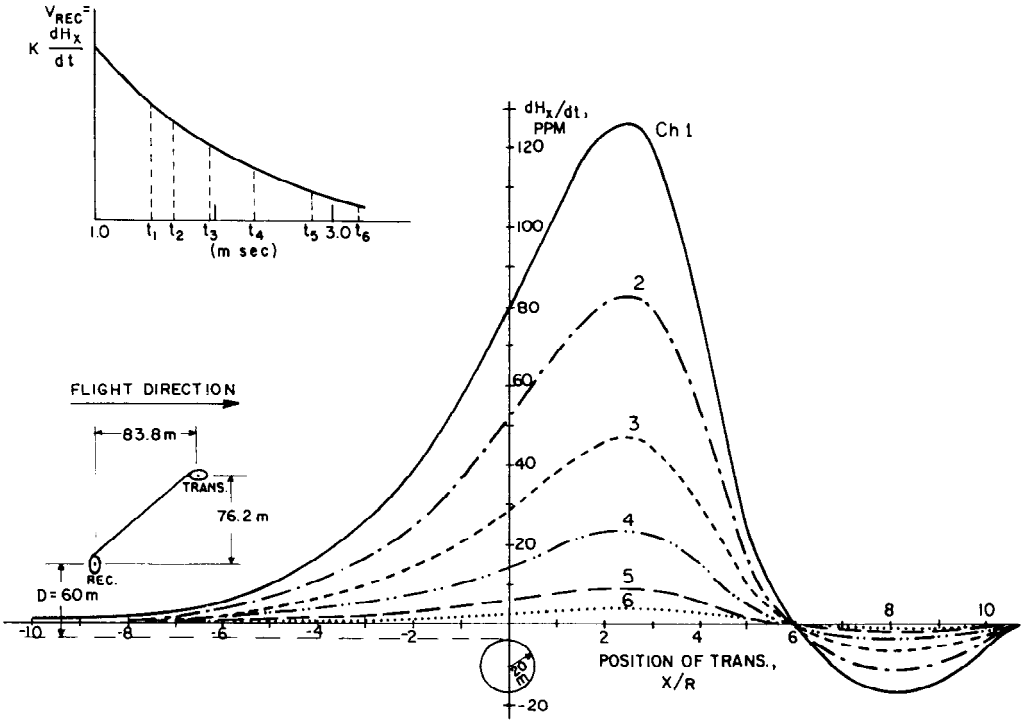

D	MAX. ANOMALY PEAK TO PEAK, PPM R=20	R=100
60	142	187
160	2.7	14.3
210	0.76	5
260	0.24	2

Ch.	CENTER TIME m sec	TIME ON msec	TIME OFF m sec
1	t_1 = 1.475	1.375	1.575
2	t_2 = 1.675	1.575	1.775
3	t_3 = 1.975	1.775	2.175
4	t_4 = 2.350	2.125	2.525
5	t_5 = 2.825	2.525	3.125
6	t_6 = 3.225	2.925	3.525

FIG. 8. Input response over test sphere.

reaching the critical field value, the field enters the wire and the wire reverts to normal conductivity. Thus, superconductors have critical currents. For pure niobium the critical field strength is of the order of 1400 gauss. For a wire 1 mm in diameter, a dc current of 425 amps could thus be supported.

Losses

In ac applications another phenomenon is manifested, particularly in type 2 super-conductors. In our description of penetrating flux lines, it must be noted that when the field is removed some of the flux lines stay in the material. They are said to be pinned, and the pinning is believed to be the result of interactions of the flux lines with the metal crystal lattice and with inhomogeneities in the alloy. Whatever the cause, the pinning process involves the dissipation of energy, very much like the energy loss in a hysteresis cycle, and this loss manifests itself as heat which can cause the superconductor to rise above its transition temperature and revert to normal conductivity. In ac applications this pinning loss phenomenon becomes of major importance and is a strong function of frequency. Periodic field reversals are constantly moving flux lines in and out of the metal with an attendant loss. The loss appears externally as a simple ohmic resistance, and the joule heating must be dissipated in the cooling medium or the wire will cease to superconduct.

The pinning process appears to be largely a materials one, in that careful alloying, use of multiple fine wire strands, and certain cold working procedures can reduce the loss. Wires have been developed which use many filaments of superconductor imbedded in a copper or copper-nickel matrix. In this case the matrix is a better thermal conductor than the superconducting alloy and so assists in dissipating the heat from the superconductor into the cooling medium.

The loss properties in ac operation are obviously a vital concern in geophysical applications. The transmitter, a coil of super-conducting wire, must be maintained below its critical temperature. For most of the alloys we considered the critical temperatures were below 10 degrees Kelvin. Thus, the only practical refrigerant is liquid helium, the boiling point of which is 4.2°K at standard pressure. Heat dissipation from ac losses is effected by vaporizing liquid helium and, consequently, reducing the volume of liquid remaining. Since the heat of vaporization of liquid helium is 20.9 joules/gm and the density of liquid helium is 0.125 gm/cc, about 4930 joules are required to boil off one liter of liquid. Over a one-hour period a liter of helium would be boiled off if the joule heating was 0.73 watts. If a large coil were refrigerated with 100 liters of helium, 50 of which could be considered as reservoir, then to achieve a ten-hour operating period between fillings the losses would have to be less than 5 liters/hour or 3.65 watts.

Quite separate from these losses, called ac wire losses, there will be a certain amount of heat transfer from the outside through the container to the liquid. This loss, a function of the insulating container or cryostat, results in a certain boil-off rate which can also be expressed in watts. We will return to considerations of cryostat design in a later section.

From practical considerations it is seen that there will be some limit imposed by the ac losses on the currents and the frequencies that might be desired. It should be noted that the single superconducting coil favors the low frequencies that we desired in the initial quest for a system with greater depth of exploration. The ac losses and, of course, coil voltage decrease with decreasing frequency allowing values of $(NA)^2$ to increase as the response falls off and at the same time maintain a sufficient dipole moment.

Wire selection

A factor in any practical design is the selection of an appropriate superconducting wire. A full description of our experiments in this regard is beyond the scope of this paper, but the basic considerations are reviewed below.

Our first studies of the experimental data on superconductors indicated that for coils of the size and moment we are considering, the magnetic field strengths would be low enough to allow the use of simple type 1 wires such as pure niobium. A series of laboratory tests using coils of niobium four inches in diameter in standard glass cryostats were conducted.

Loss values are normalized by the length of wire and the frequency and are normally presented as a function of current. There is some difficulty with this presentation since the losses are really a function of field strength as well as of length and frequency. Unfortunately, the loss appears to follow a different relationship for the self field of the wire (the field at the surface caused by current flowing in a long straight segment) than for an external field (i.e., from the other windings in a coil). The self and external fields at any point in the coil can, of course, be calculated, but it is not easy to determine experimentally what fraction of the losses is caused by a particular component of the field. This fact made it very difficult to extrapolate small coil loss data to the larger coils required for this project. Finally, the effects of frequency and field strength clearly are not linear so that each experiment required measurements at a range of frequencies and current levels, as well as the use of different coil configurations, to try to separate self and external field losses.

Our results for pure niobium wires were consistently one or two orders of magnitude higher than available data and the reason is believed to be in the different states of surface finish of the wire. We could not, as a practical matter, begin a study of surface finishing techniques so we turned to a class of type 2 wires developed for high field ac applications. We tested several multifilament niobium-titanium alloy wires in which the superconducting filaments were imbedded in a copper matrix. Our tests of this wire showed good agreement with other workers but the losses were still too high for a full scale operation. We also learned that a large percentage of the losses in a filamentary wire are due to normal eddy currents in the conductive matrix. We then tested a 0.25

mm diameter wire with 22 Nb-Ti filaments (each 0.015 mm in diameter) in a resistive copper-nickel matrix. This wire had losses which appeared to be satisfactory when roughly extrapolated to larger systems.

Test coil

We then built a 2 m diameter test coil using this wire. This coil, with the following specifications, was cooled to liquid helium temperature in the fall of 1972.

N (number of turns) = 310
D (diameter) = 2 m
$(NA)^2 = 8.8 \times 10^5$
I (maximum rms current) = 28 amps
L (inductance) = .42 henry
f_0 (operating frequency) = 40 Hz

The coil was wound with a rectangular cross-section; the winding consisted of 10 layers of 31 wires with a layer spacing of 1.9 cm and a wire spacing on each layer of .76 cm. By extrapolating small coil data, the losses were expected to be 8.4 $\times 10^{-4}$ watts/m at 40 Hz, or approximately 1.6 watts total.

The coil was installed in a fiberglass cryostat (described in the next section), brought to the superconducting state, and driven at approximately 28 amps rms. The losses were below the resolution of the helium flow meter, namely, less than 0.5 watt.

This test constituted an experimental milestone and provided a firm base for our continued research. It demonstrated that ac superconducting losses did not present a serious limitation to the development of coils suitable for geophysical prospecting.

CRYOSTATS

Introduction

Experiments with superconductors in the laboratory are usually conducted with evacuated double-walled glass (Thermos-bottle style) or stainless steel cryostats. Conductive-convective heat leak is restricted by the vacuum space, and radiation into the vessel is reduced either by metalizing the glass or by placing metalized plastic sheets in the vacuum space. The latter material is known as superinsulation and usually consists of a layer of low emissivity metal (gold, aluminum, or copper) 500 angstroms thick, vacuum-deposited on thin mylar film (6.35 microns thick). This material is placed in layers, rather loosely, so that conduction perpendicular to the layers does not become a problem and, for the same reason, the layers are separated by a thin nylon net.

In our application, eddy current losses prohibit metal cryostats and glass was considered both too difficult to fabricate and, even with sophisticated reinforcement or encasing, too fragile. This left only plastics or plastic reinforced fiber cloth. Our selection criteria were simply that a suitable cryostat had to be strong enough for an airborne system and had to be helium impermeable so that a high level of vacuum could be maintained without pumping (helium, being a small atom, tends to permeate through everything and very little gas in a vacuum space destroys its insulating property).

Fiberglass cryostats

Of the conventional fibers, glass possesses one of the best strength-to-weight ratios and this characteristic is maintained to cryogenic temperatures. Epoxy resins maintain their strength to cryogenic temperatures and when used with glass cloth that has been suitably treated, the combination displays the required high strength, resistance to thermal contraction cracking, and low permeability.

A variety of weaves and weights (ounces per square yard) of glass cloth are available as well as a bewildering array of epoxy resins. The weave determines the stretch and resulting thickness and, most importantly, the glass-to-resin ratio of the resulting laminate. A fine weave is desirable but resists resin impregnation. A compromise must ultimately be made between high cloth strength and the practical difficulty of achieving a multilayered laminate with a high glass-to-resin ratio. Areas of the laminate which have excess resin will lead to cracking upon cooling. Such cracks tend to propagate and increase the helium permeability.

Custom fabrication techniques (hand lay-up) are necessary and this results in great difficulty in achieving the requisite quality control.

While many epoxy resins are available, with as many different hardeners, detailed analyses show little variation in the cryogenic properties. An interesting feature of these combinations is that the tensile strength of the resulting solid is not severely reduced if a slightly nonstoichiometric ratio of resin to hardener is used, while an increased flexibility is obtained even at cryogenic temperatures. In some applications this feature is desirable but the interlaminar shear strength is

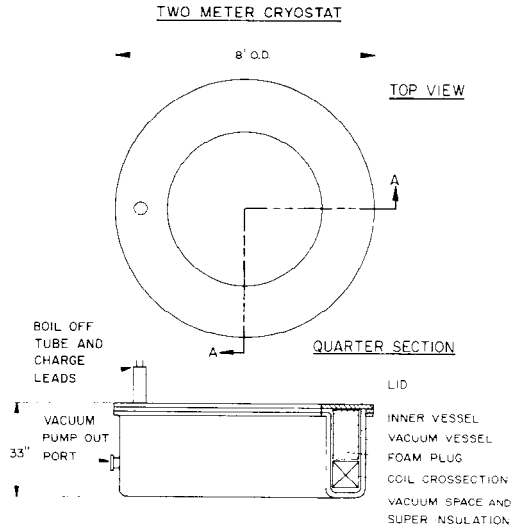

FIG. 9. Drawing of 2 m test cryostat.

reduced; so, in any portion of a cryostat that is subjected to a bending moment, this technique cannot be employed.

Test cryostats

For the 2 m diameter coil, we constructed the open mouth test cryostat shown in Figure 9. The inner vessel was constructed by hand-laying a glass epoxy resin laminate over an appropriate mold. The outer shell, not being subjected to cryogenic temperatures, was made with polyester resin and chopped glass fibers, the mixture being sprayed to a satisfactory thickness on a mold. The vacuum spaces were lined with layers of superinsulation.

It was realized that the major heat leak would be through the open mouth even though over 2 ft of insulating foam and heat shields were installed above the coil in this space. However, the necessity of conveniently accessing the coil dictated this design. [In the flight configuration, a toroidal (doughnut form) cryostat will be used and the coil must be tested thoroughly before being sealed into this unit.] The static heat leak of this test cryostat had been calculated at approximately 6 watts and the experimental results showed a value of 4 watts.

For testing a 1 m coil (the performance of which is discussed in detail in a later section), we constructed an open mouth "tub" cryostat shown in Figure 10. The vacuum space in this vessel was lined with 30 layers of superinsulation. The heat leak was 1.5 watts.

In this and other properly constructed fiberglass cryostats we have tested, we have not witnessed helium permeability.

While the open mouth cryostats require relatively thick walls to support bending moments, especially in the flanges, the walls of the inner

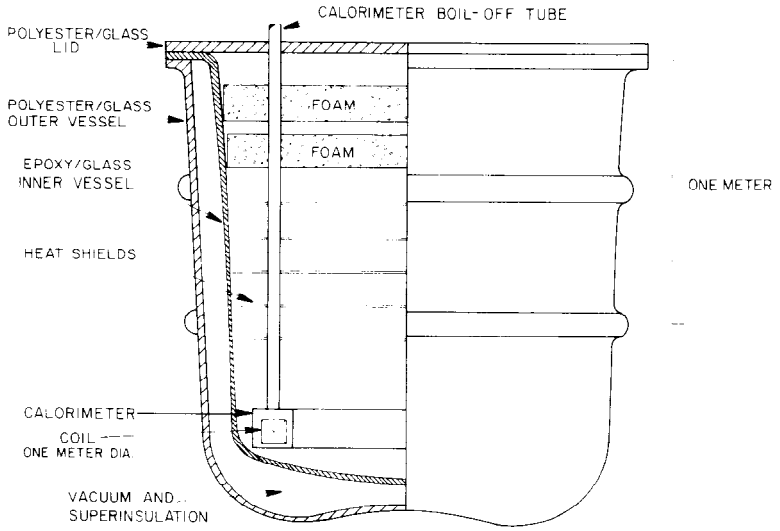

FIG. 10. Drawing of 1 m test cryostat.

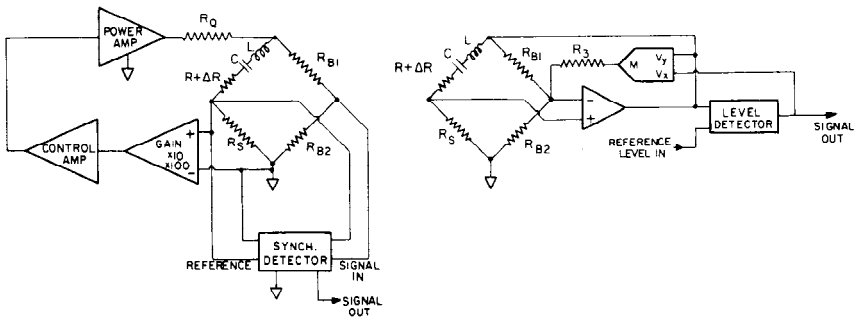

FIG. 11. Simplified schematic diagram of two unicoil measurement systems.

vessel of the 2 m cryostat were only 3.1 mm thick. This is the thickness of the inner vessel of a toroidal cryostat which will, of course, be more efficient thermally and experience only tensile or compressive stresses.

The performance of both the 1 and 2 m cryostats has shown that practical cryostats of appropriate size and weight can be constructed in a relatively straightforward manner. They have exhibited low static heat losses, no helium permeability, and adequate strength.

ELECTRONIC SYSTEMS

Bridge detector

An electronics system for measuring small changes in the resistance of the single coil has been developed by combining the coil with a series tuning capacitor. The resulting resonant circuit eliminates the reactance, and the series resistance is made up of the connecting leads, capacitor losses, ac coil losses, and the signal ΔR. These resistances constitute one arm of a conventional Wheatstone bridge allowing variations in ΔR to be monitored by measuring imbalance voltages across the detector points of the bridge. A simplified schematic of this system is shown in Figure 11a.

The time constant of the circuit is $2L/(R + Rs + R_Q)$. R_Q is a series resistance associated with the driver amplifier and may be varied at will. While the time constant of the tank itself $(2L/R)$ may be very great, leading to an impractical field situation (requiring very slow survey velocities to achieve adequate spatial resolution), the value of R_Q can be selected for any desired time constant without seriously affecting the power requirements.

Capacitors

Extraneous resistances in the LCR arm of the bridge must be minimized to take full advantage of the single coil concept. The lead resistances can be reduced, almost arbitrarily, by increasing their size; but the capacitor is a different problem. Since the requirements of a large $(NA)^2$ product and strong NIA dictate a large inductance for the coil, the operating voltages, even at the lowest frequencies desired, are in the kilovolt range. Conventional power factor capacitors in the microfarad range were found to be unsatisfactory, displaying losses well above those anticipated for the coil. A suitable set of custom capacitors was manufactured. These were made of polypropylene plastic film and aluminum foil impregnated with mineral oil. Designed to operate at up to 8000 volts at 60 Hz, the capacitors were tested at the National Bureau of Standards and found to have an equivalent series resistance of approximately 150 m-ohm at 30 Hz (see data presented in Figure 14). Since coil resistances of this same order have been measured, it appears that capacitors do not pose a serious limitation. We have, however, completed tests of polypropylene film capacitors in liquid helium and have found that such supercooled capacitors can be used to obtain even lower losses and, more importantly, thermal, and hence electrical, stability.

Noise

Noise in this system consists of: (1) instabilities in the feedback oscillator; (2) nonlinearities introduced by the feedback oscillator and driver amplifier; (3) variations in the values of the bridge resistors (principally drifts due to temperature

variations); and (4) ambient noise pick-up by the coil acting as a field detector.

Nonlinearities, which introduce spurious harmonics in the drive voltage, have little effect on the tank circuit because of its very high Q, but the harmonics appear across the balance arms of the bridge R_{B1} and R_{B2} and so, of course, are present in the detector circuit. The limiting aspect of the oscillator thus becomes fairly critical in this application. We have evolved an alternate system, which has to date performed well in laboratory tests.

Self-balancing bridge

An alternate scheme for driving the coil is shown schematically in Figure 11b. This scheme is essentially a self-balancing bridge oscillator. Again the superconducting coil L is part of a series resonant circuit, which is driven as a positive feedback oscillator. R_s is chosen to be approximately equal to the LC circuit resistance, and thus at the resonant frequency the voltage appearing across R_s is in-phase and of half the magnitude of the voltage across the LC and R_s arms of the bridge.

The voltage across R_s is then amplified by the operational amplifier A_1 whose gain is set by the resistors R_{B1} and R_{B2}. When $R_{B1} = R_{B2}$, the amplifier gain is two, and at resonance the loop gain of the amplifier and the resonant circuit is unity and the loop phase shift is zero. The conditions for oscillation are thus met and the system will oscillate. This condition is not stable since the amplitude of the oscillation will exponentially increase or decrease with any deviation from a loop gain of one.

To control the instability the amplitude of oscillation is determined and then controlled by a control loop formed by a level detector with an output control voltage (essentially, an ac to dc converter and difference integrator) and a control element (multiplier M), which controls the gain of the operational amplifier and thus the amplitude of the oscillations. The multiplier M and resistor R_3 act as a voltage controlled voltage divider. The gain of amplifier A_1 is determined in this case by the overall attenuation ratio of these elements along with R_{B1} and R_{B2}. When $R_3 > R_{B1}$ this ratio varies nearly linearly with the control voltage at the multiplier input V_x. The condition for unity loop gain means that the attenuation of the gain control must exactly equal the attenuation of the LCR series current. This condition is enforced by the control loop which sets the voltage at the multiplier in order to minimize the difference between the reference level and the output of the level detector. If the resistance of the coil changes, the control voltage must change in order to maintain constant amplitude of the oscillator. The rate of change of amplitude is a very sensitive function of the imbalance of the attenuators and so the control voltage becomes a very sensitive indicator of changes in the resistance of the LC circuit.

Both circuits have been tested in prototype form. Efforts are currently concentrated on a refined version of the self-balancing circuit (Figure 11b). Laboratory tests with breadboard circuits have shown sensitivities on the order of 10 ppm in the measurement of changes in the resistance of the tank circuit.

EXPERIMENTAL RESULTS

1 and 3 m coils

The primary goals of the research to date have been to demonstrate the principles of the single coil system and to show that practical coils and cryostats can be built which have low ac losses and, hence, low intrinsic resistances. The tests, to date, have been concentrated more on these aspects than on realizing the ultimate sensitivity of the system.

Following an experimental program of developing prototype superconducting coils, fiberglass cryostats, electronic systems, and small scale sensitivity tests with closed loop targets, we designed and built two full scale coils of 1 and 3 m diameter.

The 3 m coil design parameters are: $(NA)^2 = 1.8 \times 10^8$, $NIA = 5 \times 10^4$; operating frequency 30 to 40 Hz. This coil has been tested at liquid helium temperatures, but adverse experience with its 3 m test cryostat (similar to that shown in Figure 8) has prevented complete loss measurements and sensitivity tests.

The large cryostat for the 3 m coil presented the most costly and time-consuming challenge of the whole program. Following the success with the construction of the two meter cryostat, which we later discovered had succeeded for the wrong reasons, the construction of the larger vessel was anticipated to be straightforward. Unfortunately, the first version developed multiple cracks and leaked helium and the second collapsed under vacuum load.

Experience with the 3 m cryostat prompted exhaustive computer stress analyses and laboratory testing of the elastic and mechanical properties of various cloth-resin laminates. Application of this research resulted in a successful test cryostat for the 1 m coil, which has subsequently been through three test sequences; the results will be discussed here.

1-m coil tests

The 1-m diameter coil specifications are

N (Turns = 2185
L (Inductance) = 6.2 henries
$(NA)^2 = 2.79 \times 10^6$

23 layers in the winding cross-section.
20 turns per inch on each layer (95 turns/layer).
Wire: 30 Niobium-Titanium cores imbedded in a copper-nickel matrix (wire diameter 0.275 mm).

This coil was first cooled to liquid helium temperature in November 1974 in the test cryostat shown in Figure 10. At thermal equilibrium the cryostat exhibited a static heat leak of 1.9 watts or about 2.6 liters of helium boil-off per hour. Since most of the heat enters through the relatively poor foam insulation of the open body of the vessel, the results were very pleasing.

The coil was encased in a container, or calorimeter, within the main volume of the cryostat, which was equipped with a boil-off vent separate from that of the cryostat. This device allowed the boil-off created by ac losses in the coil to be monitored independently of the cryostat's static heat leak losses. A gas flow meter, operated in conjunction with a digital timer, permits direct reading of the calorimeter loss in watts. The meter does not function at flow rates corresponding to losses of less than 0.13 watts, although the accu-

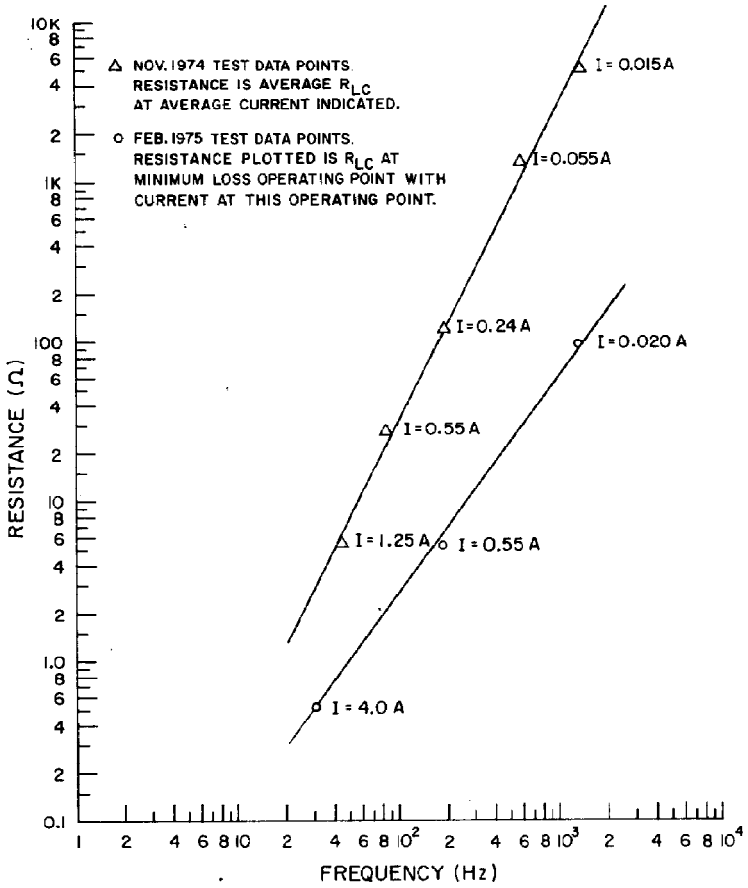

FIG. 12. Observed resistances of 1 m coil.

racy for larger flow rates is ± 0.01 watts. The flow meter is easily calibrated by dissipating a known amount of heat in a resistor immersed in helium within the calorimeter. The calibration procedure showed that the time-constant of the response of the flow meter is less than one minute. Accordingly, at least one minute of equilibration is allowed before the loss readings are recorded.

The resistance of the *LC* circuit was also measured electrically with the bridge circuitry and, more crudely, by taking the ratio of drive voltage to current. The electrically measured resistances are plotted in Figure 12 (indicated as NOV. data).

At the highest current level tested (1.25 amps rms), at 40 Hz, the boil-off losses were less than 0.13 watts, corresponding to an ac resistance of less than 30m-ohms. the electrically measured resistance at 40 Hz was approximately 5.5 ohms. The difference must reflect either eddy current losses in nearby conductors or losses in the capacitor. Since the capacitor employed was tested by NBS, and showed a series resistance of approximately 1.1 ohms at 40 Hz, the remaining resistance must lie in eddy current losses in the surroundings.

The tests were carried out at the UCB experimental field site in Richmond, Calif., where a field laboratory building (Bldg. 300) and a 100-ft high wooden tower for testing coils above the ground are available. To evaluate the effect of nearby conductors, the resistances at both 43 and 192 Hz were observed with the coil in Bldg. 300, at the base of the tower, and 3 m above ground. The results are summarized below. The current was 0.5 amps in all cases.

Frequency	Bldg. 300	Base of tower	3 m height
43 Hz	7.64 ohm	7.56 ohm	7.50 ohm
192 Hz	126.6 ohm	120.6 ohm	119.2 ohm

The ground conductivity around the tower is known to be 100 m-mho. The calculated response as the coil was lifted 3 m from the ground was about one one-hundredth of the changes observed. Clearly, the nearby metallic conductors (heavy metal compressors, coil forms, and supply cryostats in Bldg 300, and a massive steel base plate for the tower) had a large effect.

However, even the nearby metallic conductor effects could not explain the remaining high resistances at 3 m height. It was concluded that the bulk of the observed resistance was caused by eddy current losses in the superinsulation. This cryostat was insulated with 90 layers of aluminized mylar. By examining Figure 10, it can be seen that the layers were maximum coupled to the field on the bottom and upper portions of the sides. The 1 m cryostat was dismantled and reinsulated with only 30 layers employing a striped aluminized mylar.

The next test took place in February 1975 with improved electrical performance. The electrically measured resistance of the coil as a function of frequency is plotted with the previous data in Figure 12. It can be seen, for example, that at 43 Hz the resistance has dropped to 0.85 ohms from 5.5 ohms. Somewhat surprisingly, the static heat loss for the reinsulated cryostat dropped to 1.5 watts from 1.9 watts. This implies a more optimum packing of the superinsulation layers that minimizes intralayer thermal conduction.

An important point is that in the toroidal cryostats being built for the flight system the superinsulation is minimum coupled to the field, suggesting substantial reduction in superinsulation loss may be anticipated.

The wire losses were measured very accurately in this test, using the calorimeter boil-off values. The gas flow meter was biased to around one watt using the calibration resistor allowing full resolution of the meter for coil losses even below the 0.13 watt threshold. The loss data as a function of rms current level and frequency is summarized in Figure 13. The low ac wire losses indicate that helium consumption in a final airborne prospec-

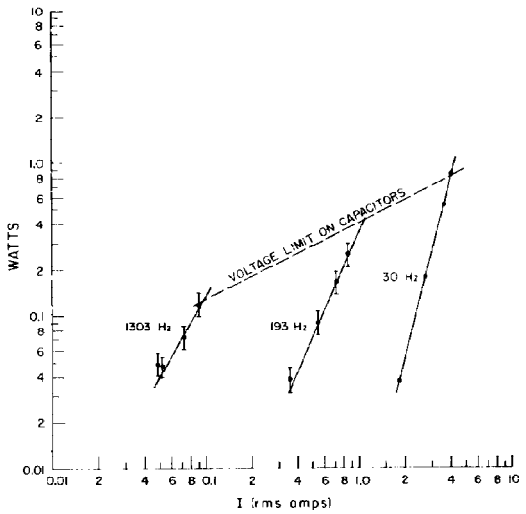

FIG. 13. Observed helium loss versus current and frequency for 1 m coil.

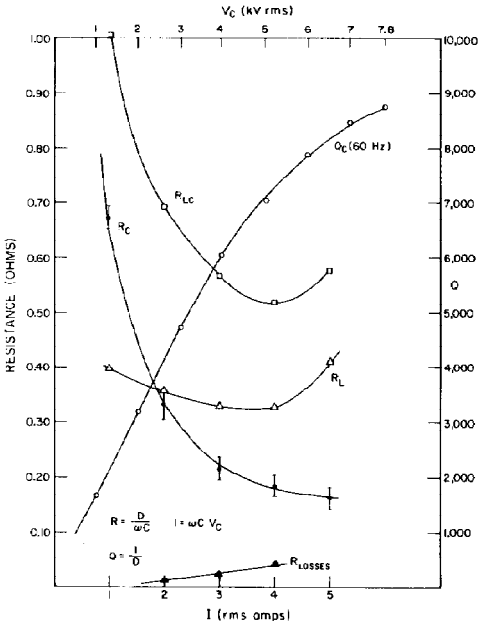

FIG. 14. Observed component resistances, 1 m coil, at 30.4 Hz.

ting system is well within practical limitations. For example, at 193 Hz and 1 amp operating level, the coil loss is approximately 0.4 watts, or approximately 0.6 liters of helium per hour. These numbers are, in fact, so low that we can contemplate a coil with a higher number of turns and a smaller cross-section, resulting in both an increase in $(NA)^2$ and a decrease in cryostat size.

The results at 30 Hz are even more encouraging. Losses of less than 1.0 watt for currents of 40 amps (Figure 13) fall well below the numbers obtained by extrapolating laboratory data from small coils. These results indicate that the 3 m coil could be constructed with an $(NA)^2$ of 3×10^8 or greater.

A summary analysis of the resistances of the various components in the LC circuit is presented in Figures 14 and 15. These figures are composites of the resistance data for the capacitors R_c, as provided by NBS (the Q of the capacitor at 60 Hz is also plotted), the overall resistance R_{LC} measured electrically, and the difference R_L, which is the effective resistance of the coil (which includes the ac losses, eddy current losses in the superinsulation, etc.). The ac losses (R_{loss}) measured calorimetrically are very small, leading to the assumption that the bulk of the coil resistance is still caused by the superinsulation. The increase in the values of R_L at high current level is not presently understood. In any event, a toroidal flight cryostat should result in an order of magnitude decrease in the superinsulation losses. Hence, the LC resistance (apparently) will be set by the series resistance of the capacitor. For the 3 m coil operating at 30 Hz, we have conservatively extrapolated a total LC circuit resistance of 0.3 ohms or less. For the 1 m coil operating at 193 Hz, the LC circuit resistance will be 1 ohm or less.

The 1 m coil can serve as an excellent prospecting system with its present characteristics. At the 1 amp operating level, the moment NIA is 1.67×10^3; the $(NA)^2$ value is 2.79×10^6, and we can safely assume an overall LC circuit resistance of 1.0 ohm. If we return to Figure 6, it can be seen that a sphere of conductivity 10 mhos/m and radius 20 m, the top of which is 30 m below the unicoil, would produce a change in resistance ΔR of approximately 1.1×10^{-11} ohms for an NA of one. For the present coil the signal would thus be $1.1 \times 10^{-11} \times 2.79 \times 10^6$, or approximately 3×10^{-5} ohms. Assuming a 1 ppm resolution in a circuit resistance of 1 ohm, this sytem would produce an electronic S/N ratio of 30. We are currently packaging this coil in a toroidal cryostat for flight tests over known targets.

To confirm the theoretical performance estimates, single turn loops of 1 and 3 m radius were

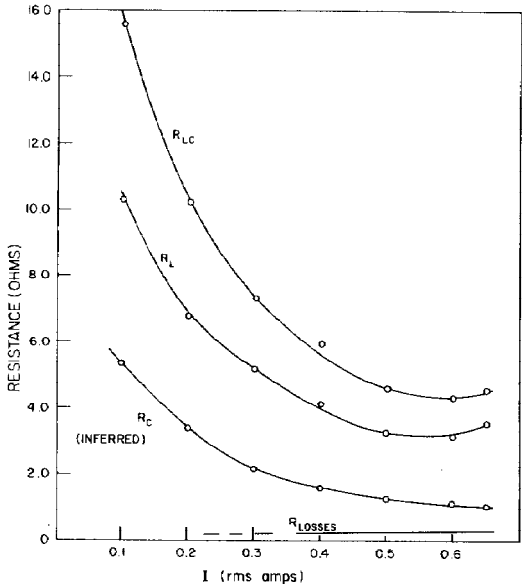

FIG. 15. Observed component resistances, 1 m coil, at 192.3 Hz.

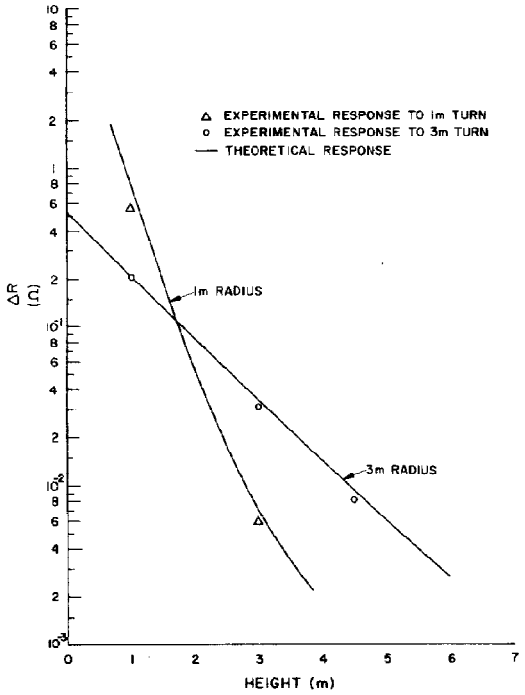

FIG. 16. Unicoil response to closed loops at 30.4 Hz, compared to calculated response.

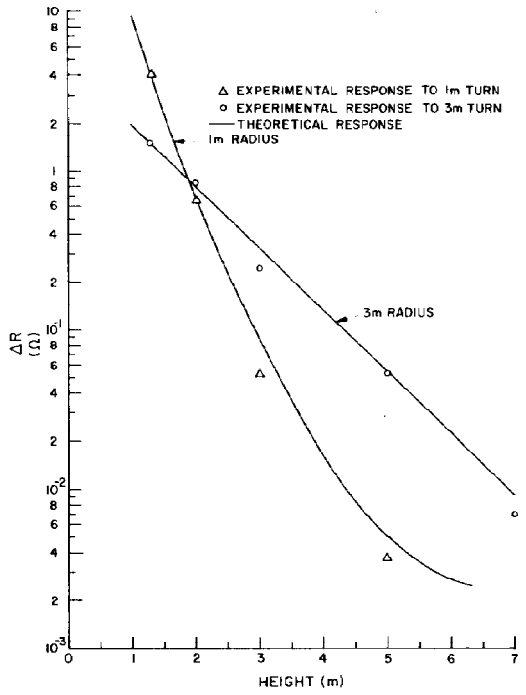

FIG. 17. Unicoil response to closed loops at 192.3 Hz, compared to calculated response

arranged on the ground coaxial to the superconducting coil. Changes in the resistance of the unicoil were observed when the single turns were individually shorted. Figures 16, 17, and 18 display the results and the calculated responses for the same shorted turns. The agreement is extraordinary at 30 Hz but less so at the higher frequencies. The ground response at higher frequencies is comparable to the coil response. Consequently, interaction of the coil with the ground cannot be ignored in the theoretical calculations as it can be at lower frequencies.

Owing to the use of deliberately versatile prototype electronics, these tests were not designed to establish the sensitivity limits of the unicoil system.

THE FLIGHT SYSTEM

Introduction

The previous sections have discussed some of the scientific and engineering developments leading to the design of a practical airborne unicoil prospecting system. Some of the design features of a system currently under construction will be discussed in the following sections.

The flight system will operate at three frequencies. Since three closely coupled coils cannot be independently driven, three separate coils in three separate doughnut-shaped cryostats will be required. The total configuration is portrayed in Figure 19. Fiberglass struts will serve as the framework that maintains the configuration. A full-scale aerodynamic model of similar size and weight has been flown and has been shown to have exceptional stability and manueverability. The largest coil is intended to operate at about 30 Hz, and the smaller coils will nominally operate at 200 Hz and 1500 Hz.

Figure 20 is designed to clarify the consideration of the choice of frequencies. A buried sphere, representative of a 1.5 million ton massive sulfide ore body, is considered. The response of a half-space is shown simply to give separately some idea of the signal level expected from the ground itself. It is not implied that the responses are additive, especially since recent scale model results actually show that the quadrature response may be increased by the presence of a surrounding less conductive half-space (Frischknecht, 1973). With this in mind, an examination of the case of the

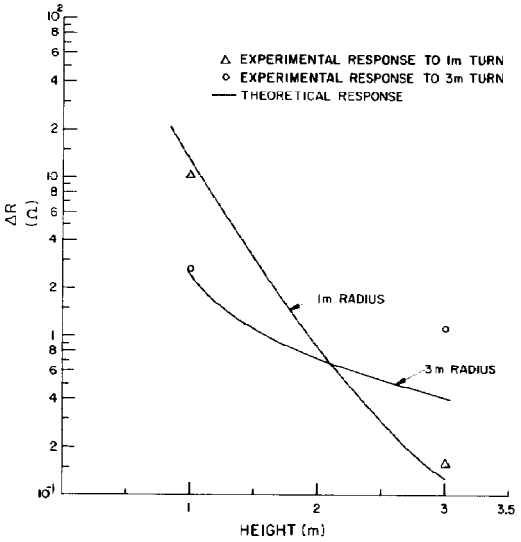

FIG. 18. Unicoil response to closed loops at 1310 Hz, compared to calculated response.

sphere centered 150 m beneath the coil in a half-space of conductivity 10^{-3} mhos/m (representative of the Canadian shield) shows that the response of the sphere at 30 Hz will be about 3 times that of the half-space and, therefore, detectable. It will probably be barely discernible at 200 Hz and not detectable at 1500 Hz. The two higher frequencies would serve for calculating the conductivity of the half-space itself.

This simple example illustrates how the frequency discrimination would apply for a rather modest ore body, 70 m beneath the surface, in a Canadian shield environment.

It should be emphasized that an important feature of the unicoil system is that it is designed to yield an absolute measurement. This is in contrast to 2-coil systems which are normally confined to relative measurements because of thermal instabilities. As a result the observed changes in resistance can be converted into apparent conductivities; that is, at a measured altitude the conductivity of a half-space that would have produced the observed ΔR can be calculated. To exploit this, a numerical scheme has been designed that reduces the three frequency data to apparent conductivities at a constant flight elevation. These data can in turn be used in an inverse program to yield the parameters of a two-layer conductivity model. The result constitutes a valuable geologic mapping tool; inhomogeneities will appear as rather bizarre, but well-defined, layer parameters.

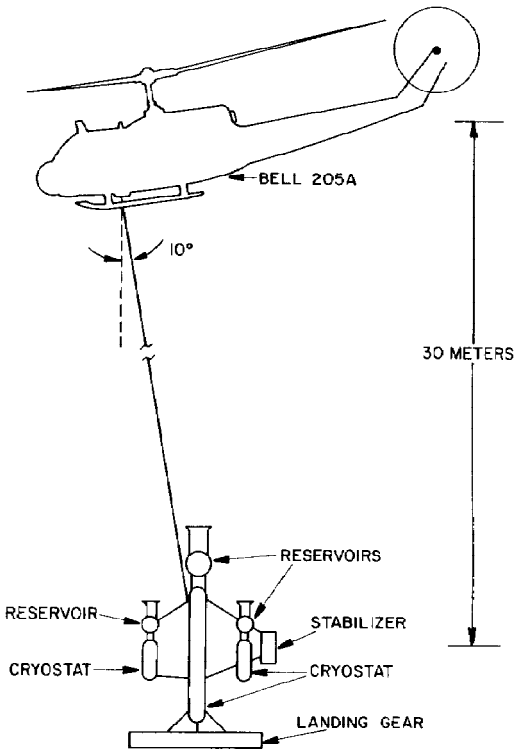

FIG. 19. Side view of unicoil flight system.

The system will be equipped with a magnetometer, photographic path recovery facilities (electronic navigation eventually contemplated), and a radar altimeter.

Data acquisition and processing

The three-frequency electromagnetic data, magnetometer, and the altimeter records present more information than can conveniently be assessed by field personnel. This has prompted the design and construction of an in-flight digital acquisition system (Figure 21) that interfaces with a field computer for data reduction and presentation. Analog channels of the coil signal voltages and currents (the latter as an indicator of system performance) are individually converted to digital form and then digitally multiplexed with the magnetometer, altimeter, and traverse line indices. These digital data are converted to a serial bit string which is recorded on a simple inexpensive analog tape recorder in a bi-phase mark format. The recorder is equipped with a read-after-write

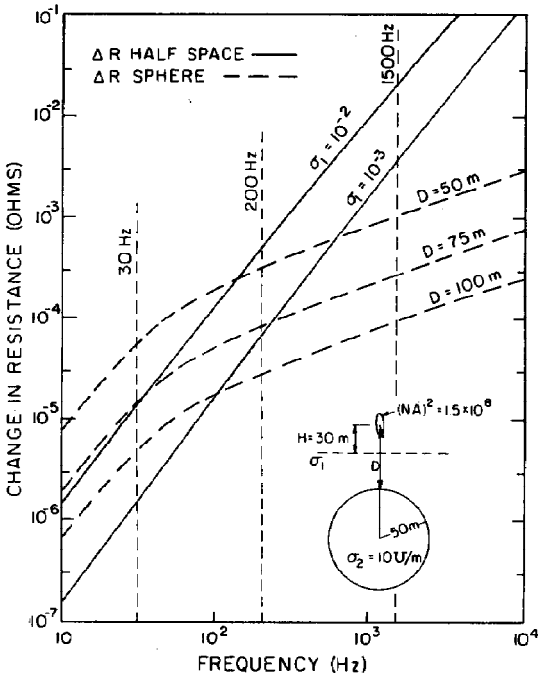

FIG. 20. Unicoil response diagram, sphere, and half-space.

head which allows in-flight analog monitoring of the data after being recorded. The analog tape is then read into the ground computer (a 20 K memory, Varian 620L) where the altitude corrections and conversion to apparent conductivities are computed. This system has been designed for reliable and fast processing and, hence, rapid evaluation of results from a fairly expensive survey system. More detailed analysis, in particular inverse solutions for specific conductivity inhomogeneities, will be effected at a large computer center.

CONCLUSIONS

The unicoil measurement system we have described has demonstrated the following advantages over existing electromagnetic prospecting systems.

1) Elimination of relative coil stability is a restraint on maximizing sensitivity.
2) The response is relatively insensitive to changes in orientation and the system can be expected to operate over rough terrain and in turbulent air.
3) The input resistance concept together with precise thermal stability provide an absolute, rather than a relative, measurement.
4) An adequate field strength to override ambient noise is obtained.
5) Frequencies of operation of as low as 30 Hz permit useful application in areas of high background conductivity.
6) Increased depths of exploration and improved conductor diagnosis are realized through a combination of inherent sensitivity, multiple frequencies, and in-field computer data processing and analysis.
7) The system is self-contained and thus does not require a dedicated helicopter.

The unicoil system also has the following disadvantages:

1) There is inherent complexity in maintaining cryogenic systems in the field.
2) The weight of the system requires a large and, consequently expensive, helicopter to transport it.
3) The only practical measurement is of the quadrature component of the secondary (anomalous) fields. However, contrary to quadrature observations with two-coil systems, the form of response with the unicoil is essentially that of the in-phase component with a 2-coil system.

The research and development work completed since September 1971 has set the stage for final engineering of the unicoil system. A 1-m coil flight system operable at 200 Hz is presently under construction and scheduled to be test flown in the near future.

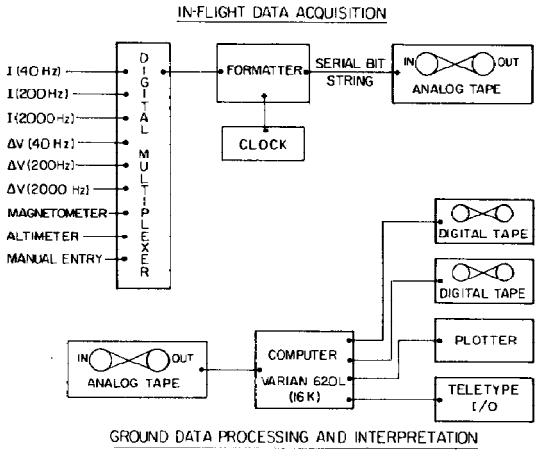

FIG. 21. Unicoil data acquisition system.

ACKNOWLEDGMENTS

This research has been supported by a grant from Amax Exploration, Inc. The research has been successful through the combined efforts of a large number of graduate students and staff in Engineering Geoscience at the University of California, Berkeley. In particular, in the initial conceptual and feasibility studies we depended upon Ben Clawson, Wayne Vogen, and Joseph Orsini. Later, in the theoretical analyses and development work we are indebted, in addition to the above, to Ugo Conti, Jim Zeitlin, Birendra Jain, Alfred Liaw, Hal Meyer, John Remenarich, and Brian Fetherstonhaugh for their contributions.

REFERENCES

Bhattacharyya, B. K., 1963, Input resistance of horizontal and vertical magnetic dipoles over a homogeneous ground: IEEE Trans. Antennas and Propag., v. AP-11, p. 261–266.

Carlson, W. L., and Hanson, E. C., 1919, Means for locating ore bodies by audio-frequency currents: U.S. patent no. 1,325,554.

Dey, A., and Ward, S. H., 1971, Inductive sounding of a layered earth with a horizontal magnetic dipole: Geophysics, v. 35, p. 660–703.

Fraser, D. C., 1972, A new multicoil aerial electromagnetic prospecting system: Geophysics, v. 37, p. 518–537.

Frischknecht, F., 1973, Model results for VLF methods: Paper presented at the 43rd Annual International SEG Meeting, October 23, in Mexico City.

Gaur, V. K., Verma, O. P., and Gupta, C. P., 1972, Enhancement of electromagnetic anomalies by a conducting overburden: Geophys. Prosp., v. 20, p. 580–604.

Grant, F. S., and West, G. F., 1965, Interpretation theory in applied geophysics: New York, McGraw-Hill Book Co., Inc.

Hohmann, G. W., 1975, Three-dimensional induced polarization and electromagnetic modeling: Geophysics, v. 40, p. 309–324.

Morrison, H. F., 1974, Electromagnetic device for determining the conductance of a nearby body: U.S. patent no. 3,836–841.

Negi, J. G., 1961, Radiation resistance of a vertical magnetic dipole over an inhomogeneous earth: Geophysics, v. 26, p. 635–642.

Ryu, J., Morrison, H. F., and Ward, S. H., 1971, Electromagnetic fields about a loop source of current: Geophysics, v. 35, p. 862–896.

Sommerfeld, A., 1949, Partial differential equations in physics: New York, Academic Press, Inc.

Terman, F. E., 1943, Radio engineers' handbook: New York, McGraw-Hill Book Co., Inc.

Wait, J. R., 1951, A conductive sphere in a time varying magnetic field: Geophysics, v. 16, p. 666–672.

——— 1953, Radiation resistance of a small circular loop in the presence of a conducting ground: J. Appl. Phys., v. 54, p. 646–649.

Ward, S. H., 1959, Unique determination of conductivity, susceptibility, size and depth in multi-frequency electromagnetic exploration: Geophysics, v. 24, p. 531–546.

——— 1967, Electromagnetic theory for geophysical application, *in* Mining geophysics, Vol. 2: SEG, Tulsa.

——— 1970, Airborne electromagnetic methods. Mining and groundwater geophysics: Proc. Canadian centennial confer. on mining and groundwater geophysics, Geol. Surv. Canada, rep. no. 26.